Title

Inhibitory Neuron Transplantation into Adult Visual Cortex Creates a New Critical Period that Rescues Impaired Vision

Authors

Davis, MF
Figueroa Velez, DX
Guevarra, RP
et al.

Publication Date

2015-05-01

DOI

10.1016/j.neuron.2015.03.062

Peer reviewed

Article

Neuron

Inhibitory Neuron Transplantation into Adult Visual Cortex Creates a New Critical Period that Rescues Impaired Vision

Highlights

- Interneuron transplantation to adult cortex reactivates critical period plasticity
- Transplantation recovers visual cortical function in visually impaired mice
- Transplantation restores normal perception to visually impaired mice

Authors

Melissa F. Davis, Dario X. Figueroa Velez, ..., Mathew C. Carathedathu, Sunil P. Gandhi

Correspondence

sunil.gandhi@uci.edu

In Brief

Davis et al. demonstrate the creation of a new critical period using inhibitory neuron transplantation into adult visual cortex. Transplantation in adulthood reverses visual impairment caused by deprivation during the juvenile critical period.

Davis et al., 2015, Neuron *86*, 1–12
May 20, 2015
http://dx.doi.org/10.1016/j.neuron.2015.03.062

CellPress

Please cite this article in press as: Davis et al., Inhibitory Neuron Transplantation into Adult Visual Cortex Creates a New Critical Period that Rescues Impaired Vision, Neuron (2015), http://dx.doi.org/10.1016/j.neuron.2015.03.062

Neuron
Article

Inhibitory Neuron Transplantation into Adult Visual Cortex Creates a New Critical Period that Rescues Impaired Vision

Melissa F. Davis,[1] Dario X. Figueroa Velez,[1] Roblen P. Guevarra,[1] Michael C. Yang,[1] Mariyam Habeeb,[1] Mathew C. Carathedathu,[1] and Sunil P. Gandhi[1,*]
[1]Department of Neurobiology and Behavior, University of California, Irvine, CA 92697, USA
*Correspondence: sunil.gandhi@uci.edu
http://dx.doi.org/10.1016/j.neuron.2015.03.062

SUMMARY

The maturation of inhibitory circuits in juvenile visual cortex triggers a critical period in the development of the visual system. Although several manipulations of inhibition can alter the timing of the critical period, none have demonstrated the creation of a new critical period in adulthood. We developed a transplantation method to reactivate critical period plasticity in the adult visual cortex. Transplanted embryonic inhibitory neurons from the medial ganglionic eminence reinstate ocular dominance plasticity in adult recipients. Transplanted inhibitory cells develop cell-type-appropriate molecular characteristics and visually evoked responses. In adult mice impaired by deprivation during the juvenile critical period, transplantation also recovers both visual cortical responses and performance on a behavioral test of visual acuity. Plasticity and recovery are induced when the critical period would have occurred in the donor animal. These results reveal that the focal reactivation of visual cortical plasticity using inhibitory cell transplantation creates a new critical period that restores visual perception after childhood deprivation.

INTRODUCTION

During a juvenile critical period, binocular vision drives the refinement of visual acuity. Deprivation of normal binocular vision during this period results in a lifelong visual deficit. Creating a new critical period in adulthood might give the visual system a second chance to rewire and recover normal vision. The maturation of inhibitory circuits in visual cortex is known to establish the timing of the juvenile critical period (Fagiolini and Hensch, 2000; Hensch, 2005; Hensch et al., 1998; Huang et al., 1999) and presents an attractive target for the reactivation of critical period plasticity in adulthood (Southwell et al., 2014).

Several manipulations of inhibition have been shown to stimulate plasticity in mouse visual cortex up to postnatal day 70 (P70) (Beurdeley et al., 2012; Fagiolini and Hensch, 2000; Kuhlman et al., 2013; Southwell et al., 2010; Stephany et al., 2014; Sugiyama et al., 2008). However, from P35 to P90, after the peak of the critical period, a weaker, qualitatively distinct form of young adult plasticity exists in mouse visual cortex (Lehmann and Löwel, 2008; Sato and Stryker, 2008; Sawtell et al., 2003). This form of young adult plasticity can be amplified with extensive training and depends upon inhibition (Fu et al., 2015). Therefore, it is possible that manipulations of inhibition boost young adult plasticity but cannot reactivate critical period plasticity.

The transplantation of embryonic inhibitory neurons into neonatal visual cortex induces new plasticity shortly after the critical period (~P45) (Southwell et al., 2010; Tang et al., 2014). Here we develop a method to transplant inhibitory neurons into adult recipient mice up to P192, long after young adult plasticity has subsided. We find that transplantation into adult visual cortex creates new plasticity that exhibits key hallmarks of the critical period.

The reactivation of critical period plasticity in adult visual cortex has the potential to reverse impairments in visual perception. Several manipulations have been used to recover visual function in impaired rodents (Kaneko and Stryker, 2014; Maya Vetencourt et al., 2008; Montey et al., 2013; Stephany et al., 2014; Tognini et al., 2012), but none have been shown to restore visual perception using a focal manipulation of plasticity in visual cortex. Here we use a behavioral test to demonstrate that inhibitory neuron transplantation restores the visual perceptual thresholds of impaired mice to normal levels.

RESULTS

Transplanted MGE Cells Disperse in Adult Cortex and Develop Molecular and Cellular Properties of Inhibitory Neurons

Neocortical inhibitory neurons are generated in the medial and caudal ganglionic eminences (MGE and CGE, respectively) of the ventral forebrain (Wonders and Anderson, 2006). First, we transplanted embryonic day 13.5 (E13.5) inhibitory neuron precursors from the MGE into adult primary visual cortex (V1). Cell placement was guided using intrinsic signal imaging to map the cortical location of primary visual cortex (V1) (Figure 1A). Transplanted MGE cells dispersed broadly through adult V1 and expressed a markerspecific to GABAergic neurons (VGAT: Figure 1B).

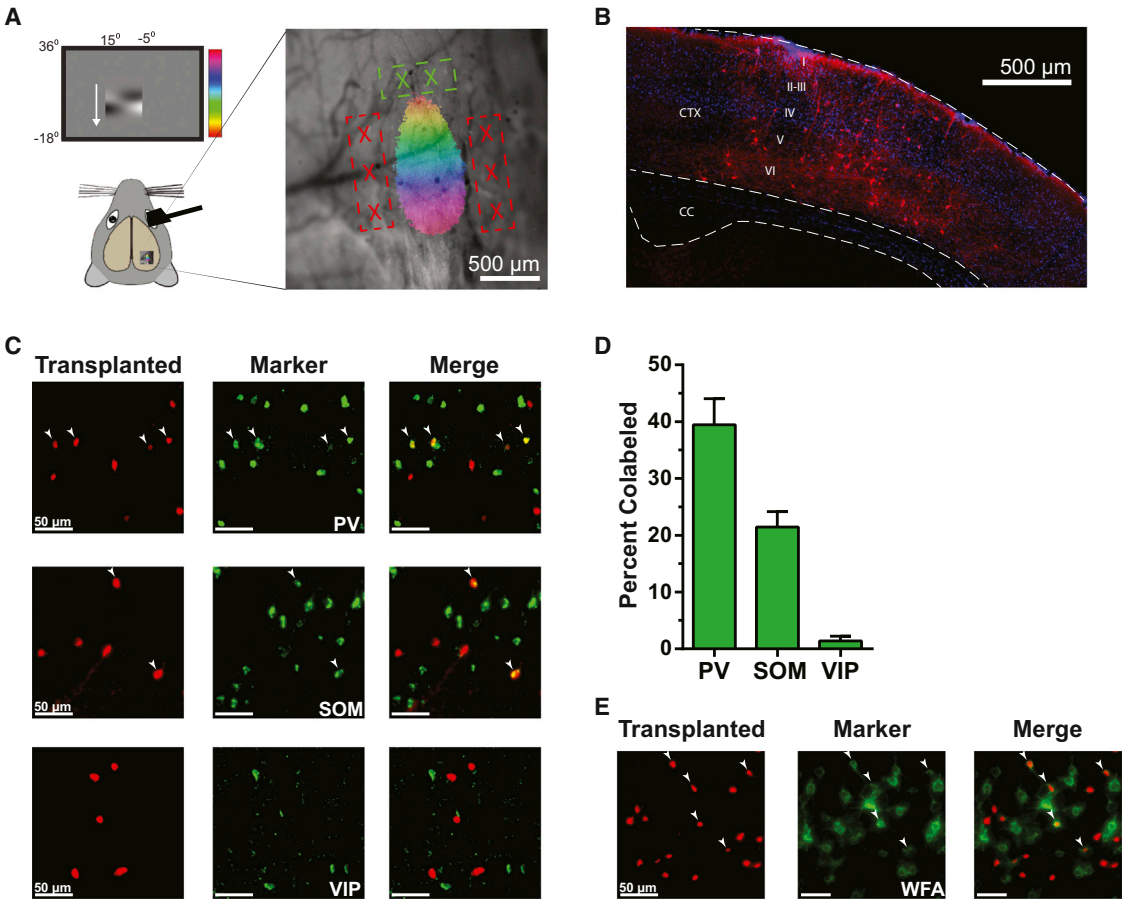

Figure 1. Transplanted Cells Migrate in Adult Visual Cortex and Express Markers of Mature Cortical Interneurons

(A) Schematic of physiologically guided transplantation to binocular visual cortex. (Right) A retinotopic map overlaid on an image of the cortical surface. Location of MGE cell injections and GCaMP6s-expressing virus injections indicated in red and green, respectively.

(B) Example coronal section from a MGE recipient 95 days after transplantation (DAT). Transplanted cells disperse across cortical layers and express the GABAergic neuron marker VGAT (red).

(C) Example transplanted VGAT-positive cells (left column) from a recipient ~100 DAT stained for Parvalbumin (PV, top row), Somatostatin (SOM, middle row), and vasoactive intestinal peptide (VIP, bottom row). White chevrons show transplanted cells expressing PV or SOM.

(D) Quantification of transplanted marker expression for PV, SOM, and VIP (n = 480 cells, n = 2 mice).

(E) Example perineuronal nets (PNNs) on transplanted cells ~100 DAT. White chevrons show transplanted cells that carry PNNs. Error is reported as SEM.

We next determined whether MGE cells transplanted into adult visual cortex developed the molecular and cellular characteristics typical of cortical inhibitory neurons. The relative proportion of Parvalbumin (PV) and Somatostatin (SOM) expressing transplanted neurons in adult recipients (39.5% PV+, 21.5% SOM+; Figures 1C and 1D) was comparable to that reported for MGE transplantation into both embryonic and neonatal recipients (Southwell et al., 2010). The laminar distribution of transplanted MGE cells also largely reproduced the profile observed in a fate mapping study of MGE cells (21.4% in L2/3 and 54.4% in L5/6; see Figure S1B online; see Pla et al., 2006). In addition, ~25% of transplanted cells developed perineuronal nets as revealed by Wisteria floribunda agglutinin staining (see Figure 1E). Together, our results suggest that transplanted MGE cells survive, disperse to appropriate locations, and develop appropriate subtypes and characteristics.

It was previously shown that MGE cells transplanted to neonatal visual cortex receive excitatory synaptic inputs (Southwell et al., 2010); however, it was unknown whether these cells developed normal sensory-evoked responses. Next, we assessed the visual response properties of fluorescently identified transplanted inhibitory cells using two-photon imaging of the genetically encoded calcium indicator GCaMP6s (Figure 2A). We focused our study on Parvalbumin-positive (PV+) neurons because of their established importance in critical period plasticity (Fagiolini et al., 2004; Hensch, 2005; Kuhlman et al., 2013) and because the visual response properties of these cells have been well characterized (Kerlin et al., 2010; Kuhlman et al., 2011; Li et al., 2012; Runyan and Sur, 2013; Runyan et al., 2010). As expected, the visual responses of transplanted PV+ cells at 91–93 days after transplantation (DAT) exhibited much broader orientation selectivity (OSI_{tPV+} = 0.39 ± 0.07, n = 11 cells) than that of neighboring, presumptive excitatory cells (OSI_{tPV-} = 0.72 ± 0.04, n = 17 cells). The

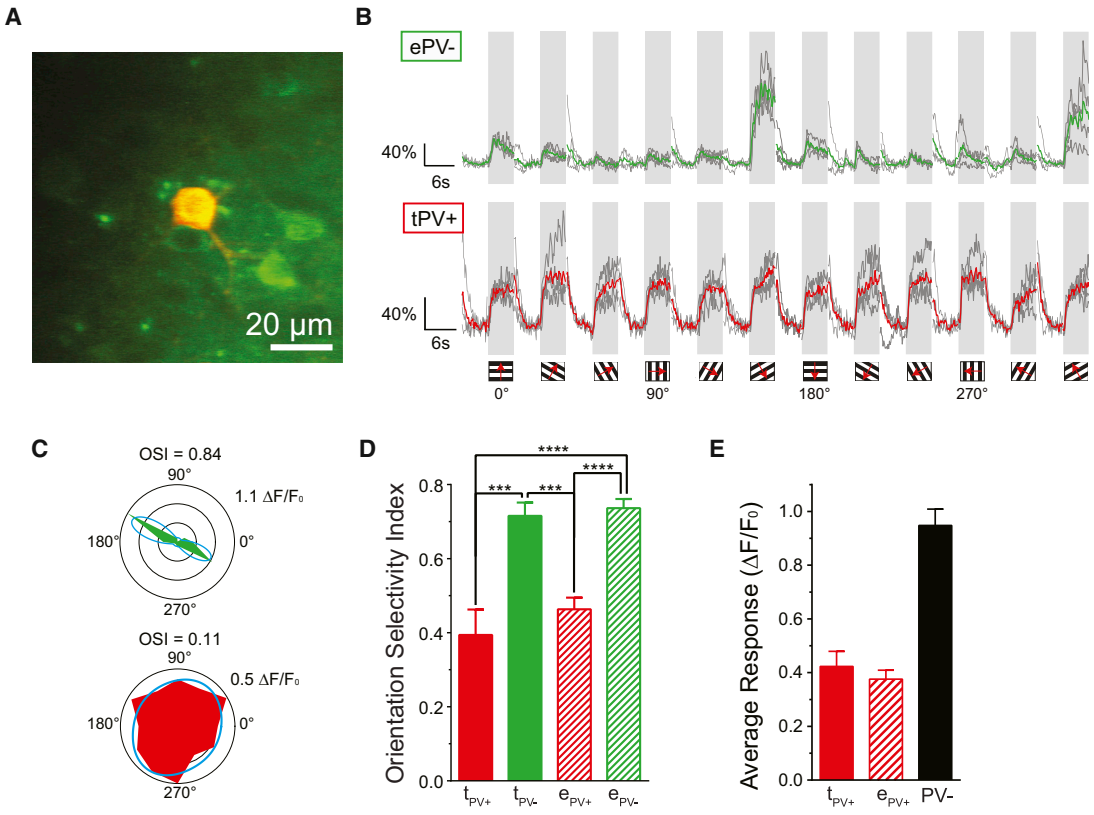

Figure 2. Transplanted Inhibitory Neurons Develop Cell-Type-Appropriate Visual Responses

(A) A transplanted PV+ (red) cell coexpressing calcium indicator GCaMP6s (green).

(B) GCaMP6s visual responses from a PV− cell (top, green) and transplanted PV+ cell (bottom, red) to drifting gratings presented at 12 different orientations (gray bars denote stimulus presentation, gray traces reflect single trial responses, red or green trace represents averaged signal).

(C) Polar plots of averaged response to stimulus orientation are shown for each example trace.

(D) Orientation selectivity of transplanted PV+ neurons (~90 DAT; t_{PV+}, solid red bar), endogenous PV+ neurons (~P140; e_{PV+}, striped red bar), and neighboring PV− neurons (t_{PV-}, solid green bar; e_{PV-}, striped green bar). Transplanted PV+ neurons have broader orientation tuning than their neighbors (OSI t_{PV+} = 0.39 ± 0.07, n = 11 versus t_{PV-} = 0.72 ± 0.04, n = 17). This orientation tuning is equivalent to endogenous PV+ cells(OSI e_{PV+} = 0.46 ± 0.03, n = 19; p = 0.78).

(E) Average response at preferred orientation ($\Delta F/F_0$) is shown for transplanted and endogenous PV+ (t_{PV+}, solid red bar; e_{PV+}, striped red bar) and PV− neurons (black bar). Responses from transplanted PV+ cells ($\Delta F/F_0$ = 0.42 ± 0.06) were comparable in strength to endogenous PV+ cells ($\Delta F/F_0$ = 0.38 ± 0.03). Error is reported as SEM.

average orientation selectivity of transplanted PV+ cells was similar to that of endogenous PV+ cells measured in untreated adult visual cortex (OSI_{ePV+} = 0.45 ± 0.03; Figures 2B–2E). Furthermore, the amplitude of the visually evoked calcium transients in the transplanted cells was quantitatively similar to endogenous PV+ cells ($\Delta F/F_0$ t_{PV+} = 0.42 ± 0.06 versus e_{PV+} = 0.38 ± 0.03). The cell-type-appropriate responses from transplanted PV+ cells suggest that these cells successfully integrated into the adult cortical circuit.

MGE Transplantation Reactivates Ocular Dominance Plasticity

In adult mice over P90, brief (<5 days) closure of one eye (monocular deprivation, MD) produces little effect on visual cortical responses (Lehmann and Löwel, 2008). In juvenile mice, brief MD strongly shifts the balance of visual responses away from the deprived eye and toward the nondeprived eye, a shift that is most pronounced during the critical period (P19–P32). To test for this ocular dominance plasticity, we used intrinsic signal imaging to measure the strength of eye-specific visual responses before and after four days of MD (see Figure 3A). An ocular dominance index (ODI) was calculated to quantify the relative strength of eye-specific visual responses. An ODI of −1 indicates that cortex responds only to ipsilateral eye stimulation, 1 indicates that cortex responds only to contralateral eye stimulation, and 0 indicates equal responses to both eyes. Four days of MD produced no discernible change in the visual responses of untreated adult mice aged P77–P113 (Figure 3B, gray; pre-MD ODI = 0.18 ± 0.02; post-MD ODI = 0.18 ± 0.02). In contrast, MD produced a robust shift in critical period mice (~P27) (Figure 3B, yellow; pre-MD ODI = 0.17 ± 0.01; post-MD ODI = 0.0 ± 0.03).

To probe for plasticity in MGE transplant recipients, we first examined plasticity 33–35 days after transplantation (33–35DAT), the time point at which the levels of critical period plasticity would have reached a peak in the donor animal

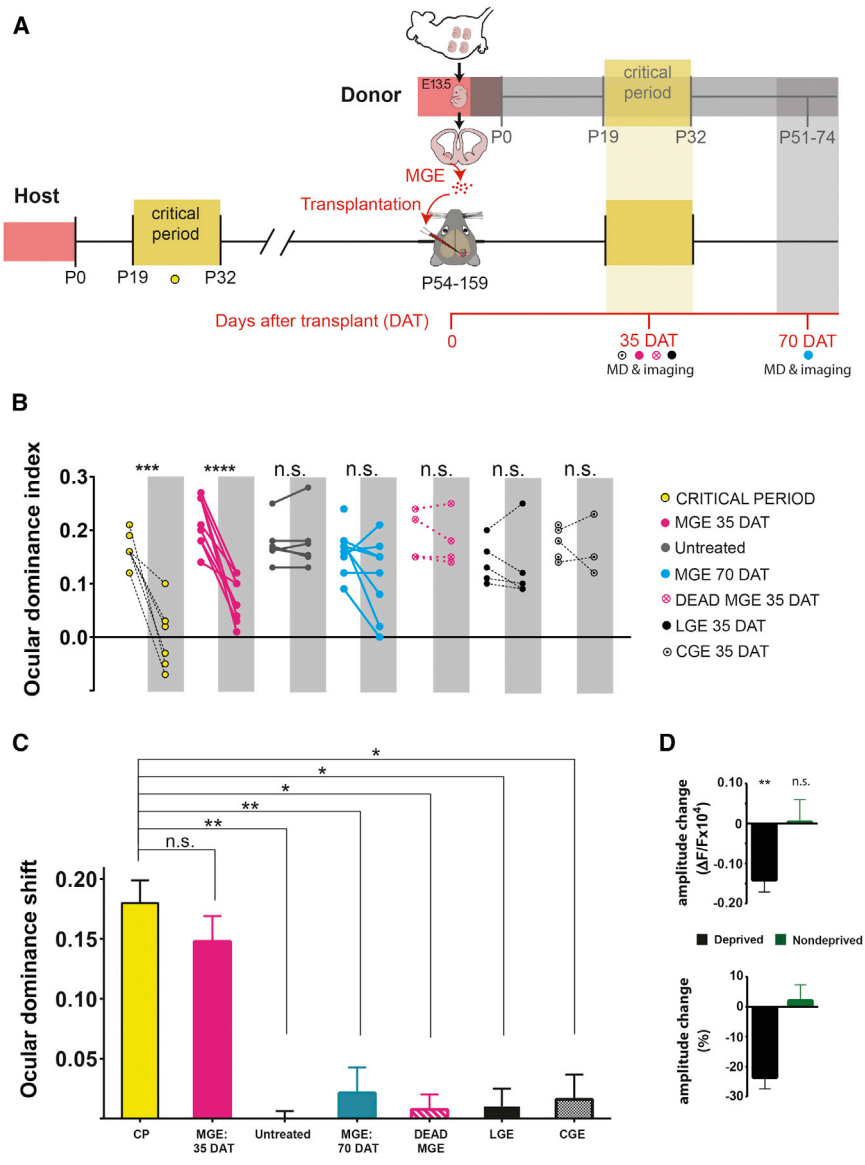

Figure 3. Transplantation Reactivates Critical Period Plasticity

(A) Timeline of the experimental protocol. Responses to contralateral versus ipsilateral eye stimulation were used to calculate an ocular dominance index (ODI). Recordings were made only in the transplanted hemisphere.

(B) Ocular dominance index determined before (white columns) and after (gray columns) 4 days of monocular deprivation (4d MD). A significant difference was seen between pre- and post-MD ODI in the CP group (yellow, n = 6: W[5] = −21; p = 0.03) and in the 35 DAT MGE group (magenta, n = 9: W[8] = −45; p = 0.004), but not in any other group.

(C) Average ocular dominance shift (ODS) following 4d MD for each experimental group in (B). ODS for MGE 35 DAT (magenta, n = 9) recipients was equivalent to critical period shifts (yellow, n = 6), but ODS in all other groups were significantly smaller than critical period ODS (versus untreated, gray, n = 7, p = 0.006; versus MGE 70 DAT, cyan, n = 8, p = 0.01; versus dead MGE, dashed magenta, n = 4, p = 0.04; versus LGE, black solid, n = 5, p = 0.03; and versus CGE, black crosshatched, n = 5, p = 0.02).

(D) (Upper graph) Four days of MD produced a loss of deprived eye visual responses (n = 8; black; t[7] = 4.83, p = 0.0019) but no significant change in nondeprived eye visual responses (n = 8; green). n.s. denotes not significant. (Lower graph) The same data shown in a plotted as a percentage of baseline amplitude. Error is reported as SEM.

(33–35 days = time span from E13.5 to ~P27). MD at 33-35 DAT (MGE 35 DAT group) resulted in a robust shift of visual responses toward the nondeprived eye (Figure 3B, magenta; pre-MD ODI = 0.21 ± 0.01; post-MD ODI = 0.07 ± 0.01). Figure 3C shows average shifts in the ocular dominance index (ODS) for each group compared to ODS for critical period animals subjected to the same 4 day MD. To rule out that the reactivated plasticity was a surgical artifact or caused by factors present in embryonic MGE tissue, we also transplanted dead MGE cells. MD did not produce a significant shift of visual responses in dead MGE cell recipients (Figure 3B, magenta dashed; pre-MD ODI = 0.19 ± 0.02; post-MD ODI = 0.18 ± 0.02), indicating that living MGE cells are needed for the reactivation of plasticity.

During the juvenile critical period, MD produces a rapid loss of deprived eye visual responses followed by a slower gain in nondeprived eye responses. In contrast, in the weeks following the critical period, MD produces a slow gain in nondeprived eye visual responses alone (Sato and Stryker, 2008; Sawtell et al., 2003). In transplantation-induced plasticity, we observed a rapid reduction in deprived eye responses (Figure 3D; post 4 day MD deprived eye versus pre: 23% reduction), with no discernible change in nondeprived eye responses. Therefore, transplantation-induced plasticity mimics critical period plasticity.

Most recipient mice were ~P65 at transplantation and were studied for plasticity at ~P100, ~2 months after the normal critical period. Two MGE recipients, however, received cells at P159 and were studied for plasticity at P192, nearly 5 months after the endogenous critical period. MD produced robust effects in these older adult recipients (Figures S3C and S3D), indicating that inhibitory neuron transplantation can reactivate plasticity up to at least 5 months after the critical period.

We observed reactivated plasticity 35 DAT, when the critical period would have been open in the donor animal (see Figure 3A). To determine whether transplantation creates a time-limited period of plasticity like the endogenous critical period, we performed MD 58–81 DAT (70 DAT group), when the critical period would have been closed in the donor animal. MD produced no significant effect at this time point (Figure 3B, cyan), in contrast to the robust shift observed in the 35 DAT group (Figure 3C,

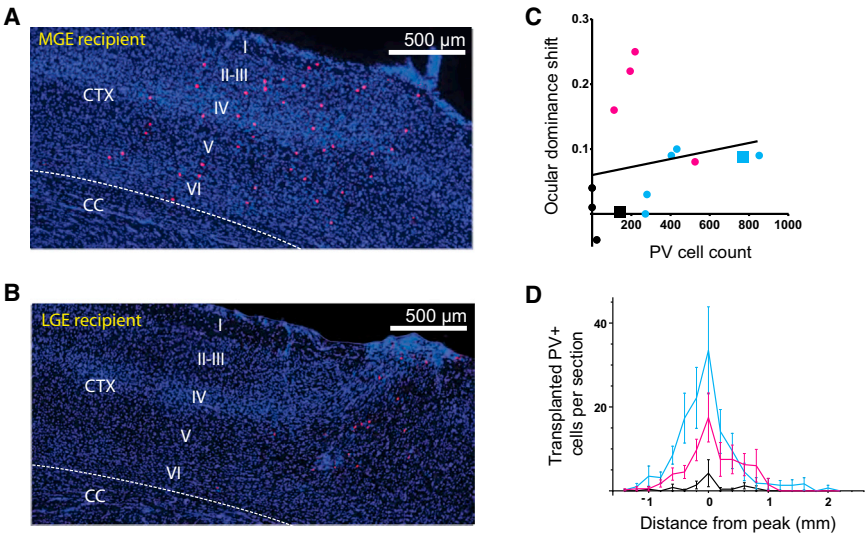

Figure 4. The Number of Transplanted PV+ Cells Does Not Predict the Extent of Plasticity

(A) An example coronal section from a MGE recipient. Transplanted PV+ cells (red) are observed in all layers of binocular visual cortex (CTX I-VI) but do not cross the corpus callosum (CC).

(B) An example coronal section from a LGE recipient; few transplanted PV+ cells were found in LGE recipients.

(C) Quantification of transplanted PV+ cells found in a subset of MGE 35 DAT (magenta), MGE 70 DAT (cyan), and LGE (black) recipients plotted against ocular dominance shifts for each animal. Square points correspond to individuals presented in (A) and (B). No relationship between ocular dominance shift and cell count was observed for MGE recipients ($R^2 = 0.042$; $p = 0.46$, n.s.).

(D) Transplanted PV+ cell spread aligned to the peak PV+ cell count position (0 on the x axis) and averaged for each group to illustrate distribution of transplanted cells. Error is reported as SEM.

magenta 35 DAT ODS = 0.15 ± 0.02 versus cyan 70 DAT ODS = 0.02 ± 0.02).

Parvalbumin-expressing (PV+) inhibitory neurons are thought to play a prominent role in the regulation of critical period plasticity (Fagiolini et al., 2004; Hensch, 2005; Kuhlman et al., 2013). It was possible that plasticity was absent in the 70 DAT group because transplanted PV+ cells died during the extended period between transplantation and assessment. We therefore compared counts of transplanted PV+ cells in a subset of recipients from the 35 DAT and the 70 DAT group (Figure 4A). There was no significant difference in the number of PV+ cells between 35 and 70 DAT MGE recipient groups. We also did not observe a relationship between the number of PV+ cells and the extent of ocular dominance plasticity (Figure 4C).

CGE and LGE Transplantation Does Not Reactivate Plasticity

To determine whether another source of cortical interneurons could produce ocular dominance plasticity, we transplanted cells from the caudal ganglionic eminence (CGE). CGE cells also expressed markers specific to GABAergic neurons, but dispersed in the adult neocortex less extensively than MGE cells (VGAT, Figure S1A). CGE transplantation did not induce any detectable plasticity at 35 DAT (Figure 3B, black dashed; pre-MD ODI = 0.18 ± 0.01; post-MD ODI = 0.17 ± 0.03). In contrast to MGE cells, CGE cells transplanted into adult visual cortex adopted a laminar distribution that differed substantially from the normal fate of these cells by skewing to the deeper layers (71.6% in L5/6; Figure S1B; 20%–30% in L5/6 [Miyoshi et al., 2010; Pla et al., 2006]).

Whereas the medial and caudal ganglionic eminence produce cortical interneurons, the lateral ganglionic eminence (LGE) produces interneurons destined for the olfactory bulb and striatum. MD produced no effect in adult LGE recipients (Figure 3B, black solid; pre-MD ODI = 0.14 ± 0.02; post-MD ODI = 0.13 ± 0.03). As expected, transplanted LGE tissue largely failed to disperse in the adult visual cortex (Southwell et al., 2010; Wichterle et al., 1999) A small number of PV+ cells were occasionally found in LGE recipients, however, likely due to a small amount of contamination from MGE originating cells (Figure 4B, lower panel). Nonetheless, these cells did not induce plasticity (Figures 3B and 3C).

Taken together, these results demonstrate that the transplantation of live, MGE-derived inhibitory neurons creates a new critical period of plasticity in adult visual cortex.

Recovery of Visual Cortical Function

In our next set of experiments, we sought to recover cortical function in visually impaired animals using transplantation-induced plasticity. MD that spans the critical period produces a permanent disruption of visual cortical responses to the deprived eye. We transplanted inhibitory neurons to and assessed effects in the cortex contralateral to the previously deprived eye. As a control, visual responses in the opposite hemisphere were recorded in response to stimulation of the nondeprived eye (Figure 5A).

We used intrinsic signal optical imaging to assess the impairment of cortical responses prior to the reactivation of plasticity, 0–24 DAT (15 DAT). To probe for recovery, we then reassessed the same animals after reactivation of plasticity, at 47–62 DAT (55 DAT) (Figure 5). Figure 5B shows example intrinsic imaging responses to drifting noise stimulus. The deprived eye retinotopic map reveals a particularly severe deficit (Figure 5B, black, 0 DAT). By 48 DAT, however, the deprived eye retinotopic map has recovered (magenta).

We then assessed responses in primary visual cortex to stimuli across a range of spatial frequencies in order to provide a neurophysiological measure of visual acuity (Beurdeley et al., 2012; Heimel et al., 2007; Sugiyama et al., 2008). Response values were normalized as a percentage of the maximum response produced by stimulation of the nondeprived eye. Figure 5C shows cortical responses for the severely impaired mouse in Figure 5B

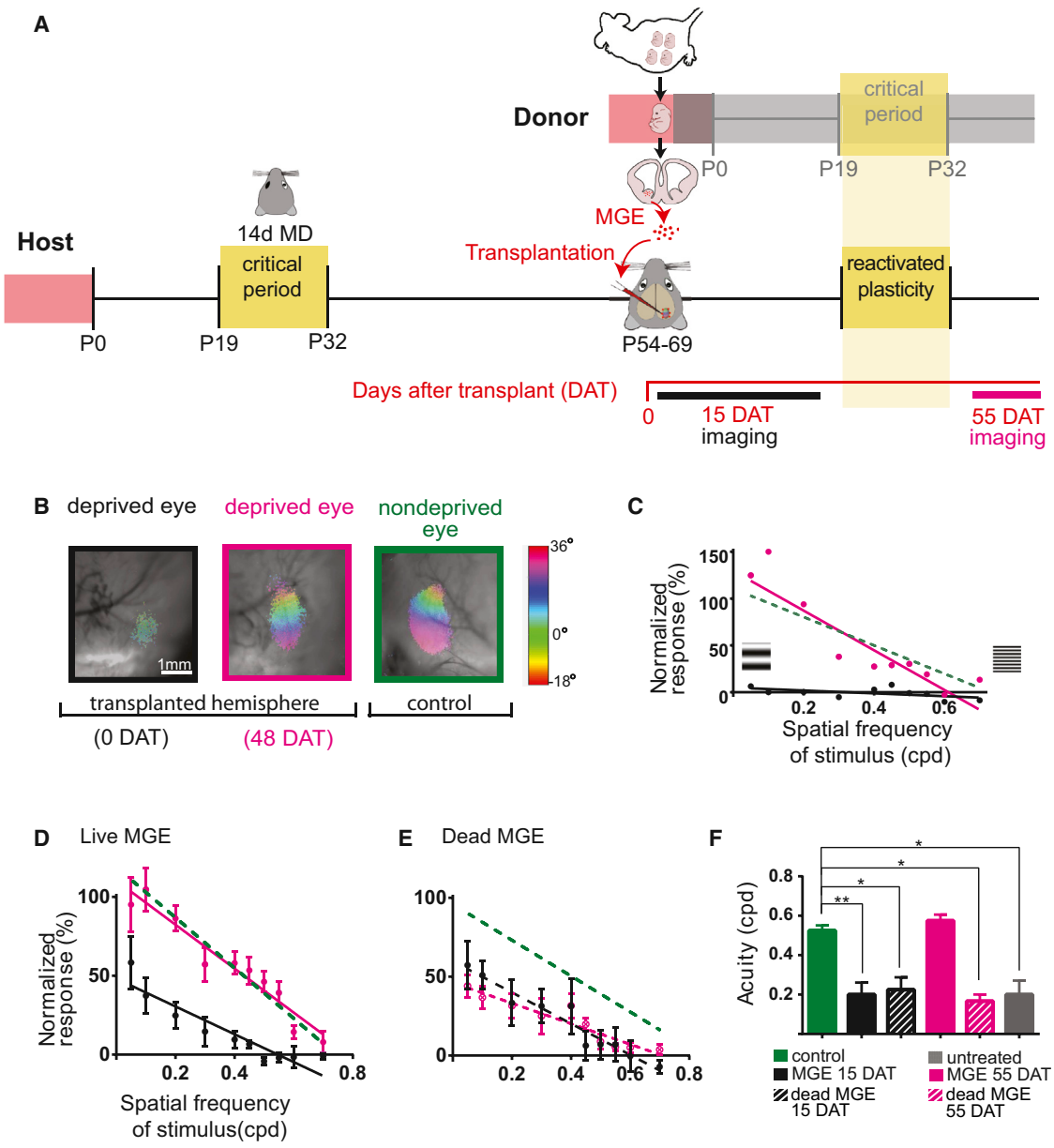

Figure 5. Transplantation Reverses Cortical Effects of Visual Deprivation during the Critical Period

(A) Timeline of the experimental protocol. Only responses to contralateral eye stimulation were recorded from each hemisphere.

(B) Retinotopic maps for an example animal. From left to right: deprived eye 0 DAT (black) and 48 DAT (magenta), and nondeprived eye (green). Scale bar denotes visual field elevation.

(C) For animal from (B), cortical responses to visual stimuli across a range of spatial frequencies presented to the deprived eye at 0 DAT (black) and 48 DAT (magenta), and responses from the control (nondeprived) eye (green dashed line)

(D) Average deprived eye responses at 15 DAT (black, n = 6) compared to 55 DAT (magenta, n = 5); Lines differ significantly: ANCOVA, $p = 0.01$. Control eye responses for this group shown as green dashed line

(E) Average deprived eye responses at 15 DAT (black, n = 3) and 55 DAT (dashed magenta, n = 3) in dead MGE transplant recipients; lines do not differ significantly. Control eye responses for this group are shown as green dashed line.

(F) Average acuity of visual responses to stimulation of deprived and nondeprived eyes in live and dead MGE recipients as well as untreated animals differed across groups $H = 28.35$, $p < 0.0001$. Compared to nondeprived control eye (green, n = 18) acuity, deprived eye acuity of live MGE (black solid, n = 7) and dead MGE (black striped, n = 4) recipients at 15 DAT was poor ($p < 0.002$ and $p < 0.05$, respectively). By 55 DAT, deprived eye acuity recovered to nondeprived eye levels in live MGE (magenta, n = 5), but not dead MGE (magenta, stripes; n = 3; $p < 0.05$) recipients. No spontaneous recovery was observed in untreated impaired animals (gray, n = 4, $p < 0.03$). Error is reported as SEM.

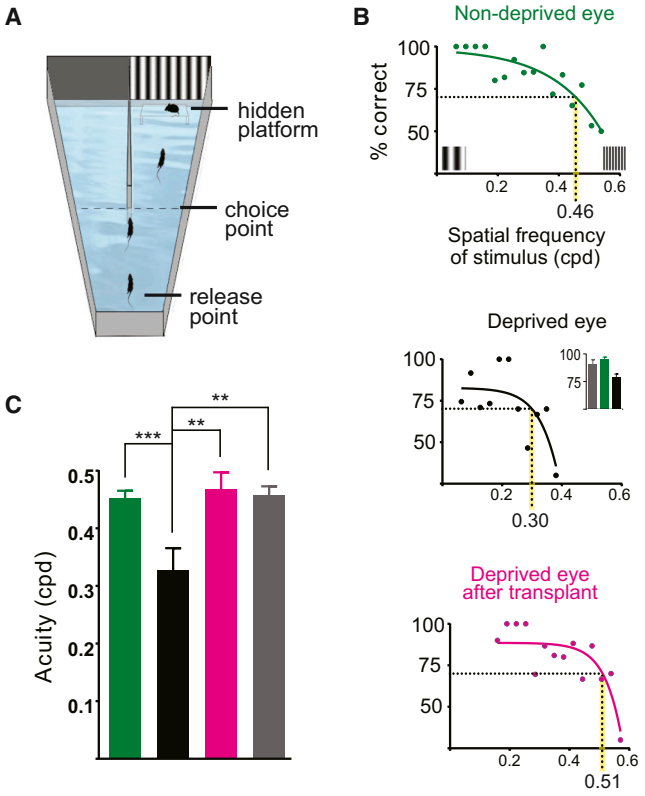

Figure 6. Transplantation Reverses Perceptual Deficits in Visually Impaired Animals

(A) Schematic of the visual water task.

(B) (Top) Representative performance on a visual task for (top) a mouse using the nondeprived eye (green), acuity threshold = 0.46 cpd (gradings on x axis schematically represent the spatial frequency of the visual stimulus); (middle) an untreated mouse using the deprived eye, acuity threshold = 0.30 cpd. Inset graph compares the maximum performance by untreated animals through deprived (black) and nondeprived (green) eyes versus normally sighted animals (gray). (Bottom) A MGE recipient mouse using the deprived eye for the visual task, acuity threshold = 0.51 cpd.

(C) Quantification of perceptual acuity across groups ($F_{(3,\ 37)}$ = 7.52, p = 0.0005). MGE recipients tested using the deprived eye (n = 5, magenta) had acuity equivalent to that of deprived animals using the control (nondeprived) eye (n = 18, green) and to that of naive animals (n = 9, gray). Untreated, impaired animals tested using the deprived eye (n = 9, black) had significantly depressed acuity thresholds compared to MGE recipients (p = 0.007), nondeprived eyes (p = 0.0008), and naive animals (p = 0.003). Error is reported as SEM.

at 0 DAT (black) and 48 DAT (magenta). At 0 DAT, no response was observed at any spatial frequency. Strikingly, by 48 DAT, responses to deprived eye stimulation were restored to levels equivalent to responses to nondeprived eye stimulation (green dashed line). For all live MGE recipients, we observed marked deficits prior to reactivation of plasticity (15 DAT; Figure 5D; black). After the reactivation of plasticity (55 DAT), however, visual responses improved significantly (p = 0.01; Figure 5D; black versus magenta) to levels indistinguishable from the nondeprived eye (dashed green line).

We also examined the effects of transplanting dead MGE cells to the cortex of visually impaired mice. In the previous MD experiments, no plasticity was observed at 35 DAT in dead MGE recipients (Figures 3B and 3C). As expected, at 55 DAT, visual responses to the deprived eye remained unchanged compared to 15 DAT (Figure 5E). We also assessed untreated visually impaired animals to test for spontaneous recovery. These untreated animals were assessed up to ~5 months after initial deprivation and showed no sign of recovery (acuity, 0.20 ± 0.07 cpd; Figure 5F, gray).

To assess thresholds of acuity in cortical responses, we determined the spatial frequency of the visual stimulus at which responses fell to background levels. Figure 5F shows that at 15 DAT, average acuity for the deprived eye responses in both live and dead MGE recipients is significantly lower than for nondeprived eye responses (0.20 ± 0.16 cycles per degree [cpd] for MGE recipients, n = 7; 0.23 ± 0.13cpd in dead MGE recipients, n = 3; versus 0.52 ± 0.11cpd in nondeprived eyes, n = 18; p = 0.0015 and p = <0.05, respectively). By 55 DAT in live MGE cell recipients, average acuity for the deprived eye reached threshold levels indistinguishable from the nondeprived eye (0.52 ± 0.11cpd versus 0.59 ± 0.07 cpd). In contrast, at 55 DAT in dead MGE cell recipients (n = 3), results were unchanged compared to 15 DAT and matched untreated impaired mice (n = 4) (0.17 ± 0.06 cpd versus 0.23 ± 0.13 cpd, versus 0.20 ± 0 cpd.14; Figure 5F).

It was possible that the migration of transplanted cells through the host cortical tissue initiated recovery. If this were the case, we would expect to see improvements in cortical responses by 14 DAT, when the cells complete their migration in the host brain. Figure S5 shows that even by 19–24 DAT, the acuity of cortical responses has not yet improved. These data suggest that the observed recovery of cortical function produced by inhibitory neuron transplantation comes after cell migration is completed.

Taken together, these results show that inhibitory neuron transplantation reverses the impairment in deprived eye cortical responses (Figure 5). However, it remained possible that visual perception through the deprived eye remained impaired despite the restored acuity of visual cortical responses (Stephany et al., 2014).

Restoration of Visual Perception

Next, we tested the ability of transplant recipients to see through the deprived eye and nondeprived eye using a visual water task (Prusky et al., 2000). Mice learned to associate a hidden escape platform with a visual grating (Figure 6A). Mice were then challenged to find the platform with visual gratings of increasing spatial frequency to determine the perceptual limit of their vision. Acuity through the deprived and nondeprived eyes was assessed independently by covering one eye during testing. We tested three groups: visually impaired mice that received live MGE cells, untreated impaired mice, and normally sighted mice. Recipient mice were trained on the task starting at 31 DAT, along with age-matched controls. Perceptual thresholds for vision through the nondeprived eye of each mouse were also assessed. The average threshold for vision through the nondeprived eye was 0.45 ± 0.01cpd, equivalent to that of normally sighted controls (0.46 ± 0.02 cpd) and consistent with published data (Prusky and Douglas, 2003) (for representative cases, see Figure 6B). Thresholds for untreated impaired mice using the

deprived eye were significantly lower (0.33 ± 0.04 cpd; p = 0.0008 versus nondeprived eye; p = 0.003 versus normally sighted controls; Figure 6C). The same mice, however, performed the task using their nondeprived eyes as well as normally sighted animals. Therefore, the visual deficit in the impaired mice was specific to the deprived eye. In contrast to untreated impaired mice, MGE recipients fully recovered vision through the deprived eye (0.47 ± 0.03 cpd; Figures 6B and 6C). These results make clear that inhibitory neuron transplantation reverses the visual deficit imposed by MD during the endogenous critical period.

DISCUSSION

In light of our findings, we conclude that the transplantation of inhibitory neurons into the adult visual cortex creates a new critical period. Four lines of evidence support this conclusion: (1) Transplantation induces ocular dominance plasticity at 35 DAT when the critical period would be open in the donor animal, but not at 70 DAT when the donor critical period would be closed. (2) The level of ocular dominance plasticity induced by transplantation is quantitatively similar to normal critical period plasticity. In addition, transplantation induced plasticity is equivalent to that induced by diazepam treatment before the critical period (~P18–P22; data not shown). (3) The transplant-induced recovery of visual acuity in visually impaired adult mice begins after 25 DAT and is complete by 45 DAT, when the donor critical period would be closed. (4) Brief MD during the transplant-induced critical period produces a loss of deprived eye input, a hallmark of critical period and not adult plasticity.

It is striking that transplanted MGE cells migrate to the appropriate cortical layers in adult tissue. In contrast, the cortical layer distribution of transplanted CGE cells raises questions about migration cues (Figure S1). Unlike for transplanted CGE cells, distributions of transplanted MGE cells in our experiments were similar to those previously reported in MGE fate-mapping studies (~54% in layers 5/6 and ~21% in layers 2/3). Perhaps the migration of MGE cells is guided by intrinsic migration cues, while CGE-derived cells require external developmental cues from the neonatal brain.

It is also intriguing that transplanted cells acquire normal visual response properties (Figure 2). There is some recent evidence that the orientation selectivity of PV+ neurons in the visual cortex may be heterogeneous, with some sharply tuned and other broadly selective cells (Runyan and Sur, 2013). Future studies may address any functional heterogeneity of transplanted cells in particular once new genetic markers become available for parceling out subpopulations of PV+ cell types.

It is remarkable that the transplantation of embryonic inhibitory neurons is sufficient to restore visual function in primary visual cortex without any explicit sensory training. Various manipulations of sensory environment or experience coupled with physical activity have been shown to recover visual function (Kaneko and Stryker, 2014; Montey et al., 2013; Tognini et al., 2012). These manipulations, however, are likely to have widespread effects in the brain. In contrast, transplantation of inhibitory neurons provides a focal manipulation because the transplanted cells do not spread beyond visual cortex.

Further investigation of different properties of transplanted MGE and CGE cells may yield insight into the mechanisms of transplant-induced plasticity. For example, in fate-mapping studies, cells from CGE predominately migrate into cortical layers 2 and 3 (Miyoshi et al., 2010). In contrast, most cells from our CGE transplants were found in layers 5 and 6, with a very small fraction found in layer 2. The lack of transplanted CGE cells in the superficial layers of cortex may have prevented the induction of plasticity.

In addition, a detailed study of the cell types contributed by MGE versus CGE transplantation may shed light on the mechanisms of the critical period. A dominant hypothesis is that PV cells are critical to the induction of plasticity (Hensch, 2005). In our study, however, we found that the number of transplanted PV+ cells from the MGE did not predict the extent of induced plasticity in adult recipients. This finding agrees with earlier transplantation studies in neonatal mice that find no obvious relationship between the reactivation of plasticity and the number of PV+ cells (Southwell et al., 2010; Tang et al., 2014). Moreover, a recent publication shows that the depletion of both PV+ and SOM+ transplanted cell populations prevented plasticity induction, but that the ablation of either population independently did not prevent plasticity (Tang et al., 2014).

Interestingly, while the addition of new interneurons to the cortex induced a new critical period in adults, diazepam does not induce plasticity in adults (data not shown; Fagiolini and Hensch, 2000). Therefore it is unlikely that increased inhibition results in plasticity following MGE cell transplantation. How then do transplanted cells induce such extensive plasticity in the adult? Perhaps the addition of young interneurons weakens endogenous inhibition, allowing developmental plasticity to occur for a second time. Another possibility is that the transplanted cells have little effect on endogenous inhibition and enact their own intrinsic program for critical period plasticity. Future experiments are needed to assess the physiological changes to endogenous and transplanted cells during the induced critical period.

Inhibitory neuron transplantation provides a novel means to investigate the developmental mechanisms that create the critical period. There is evidence that factors expressed at the onset of the critical period trigger the maturation of inhibitory circuits and set the timing of the critical period (Beurdeley et al., 2012; Sugiyama et al., 2008). If the adult brain were no longer expressing these factors, transplantation should not produce plasticity. However, if these factors remained present in the adult, transplantation should have produced plasticity earlier than we observed. Instead, Our findings suggest that the mechanism responsible for producing the timing of the critical period is contained within inhibitory neurons. This observation suggests that extrinsic developmental factors are permissive, not instructive, for the induction of critical period plasticity.

To our knowledge, this is the first demonstration that a focal reactivation of plasticity in the cortex fully restores visual perception in impaired mice. Further, these results reveal that factors intrinsic to inhibitory neurons from the MGE are responsible for creating the critical period. Inhibitory neuron transplantation offers a promising avenue for reorganizing the brain after injury or disease. It also provides a broadly applicable new tool for exploring the logic of postnatal development.

EXPERIMENTAL PROCEDURES

Animals

All protocols and procedures followed the guidelines of the Animal Care and Use Committee at the University of California, Irvine. Embryonic donor tissue was produced by crossing CD-1 wild-type mice with homozygous mice expressing red fluorescent protein tdTomato in either Parvalbumin (PV+) cells (PV-tdT, PV-Cre) (Hippenmeyer et al., 2005) X (LSL-tdTomato) (Madisen et al., 2010) or VGAT+ cells (Vong et al., 2011) (VGAT-tdT, VGAT-Cre;LSL-tdTomato). Wild-type C57/BL6 host mice and CD-1 breeder mice were obtained from Charles River Laboratories. All mice were housed individually from experiment onset.

Tissue Dissection

The medial or lateral ganglionic eminence (MGE or LGE) was dissected from embryonic day 13.5 (E13.5) PV-tdT (adult MD experiments) or VGAT-tdT (visual deficit rescue experiments) embryos as previously described (Southwell et al., 2010). Caudal ganglionic eminence (CGE) was dissected at E13.5 from VGAT-tdT embryos by taking approximately the caudal third of the ganglionic eminence. Detection of a sperm plug was used to define E0.5. Explants were maintained in chilled L-15 medium with 15 mM HEPES buffer until transplantation. For dead MGE, cells in L-15 underwent three cycles of freeze-thaw (3× −20°C to 100°C) and were stored at −20°C until transplantation.

Retinotopic Map-Guided Cell Transplantation

A map of binocular visual cortex was obtained using intrinsic signal imaging (described below; also see Figure 1A). This map guided the placement of skull slits medial and lateral to binocular visual cortex using a dental drill (Midwest 78044) and FG1/4 carbide burr (see Figure 1A, red dashed rectangles). Cells were loaded into a beveled glass micropipette (~75 μm tip diameter; Wiretrol 5 μl, Drummond Scientific Company) using a custom-designed hydraulic injection apparatus. The micropipette was positioned at a 45° angle to the cortical surface and advanced axially ~700 μm into the cortex. Injections of cells ~15–20 nL (~2,000 cells/nL) were made at three locations along each slit; totaling 6× ~15–20 nL and ~12,000 cells per host animal (see Figure 1A). The scalp was then sutured, anesthesia was terminated, and the animal was placed on a warm surface until mobile.

Monocular Deprivation

During critical period or adult MD, if an eye opened prematurely or was found to be damaged, the animal was excluded from the study. For ocular dominance plasticity experiments, the eyelid contralateral to the site of transplantation was closed for 4 days using two mattress sutures (7-0 silk, Ethicon) and checked daily. To produce visual deficits, One eyelid was closed using one silk mattress suture. This closure was maintained for the duration of the normal critical period (~P18–P32) and was checked daily (Prusky and Douglas, 2003). If signs of suture fraying were observed, a small drop of tissue adhesive (60% 2-octyl and 40% N-butyl cyanoacrylate; GLUture) was applied to the suture knot.

Surgical Preparation

All mice were anesthetized with isoflurane in O_2 (2%–3% for induction; 1.5% for surgical procedures; 0.6%–0.9% for imaging). During imaging sessions, anesthesia was supplemented by a single intraperitoneal injection of chlorprothixene (1 mg/kg). Atropine (0.3 mg/kg SQ) and carprofen (5 mg/kg) were administered subcutaneously to reduce secretions and to provide analgesia, respectively. For experiments lasting 3 or more hours, 0.15 mL saline was administered every 1–1.5 hr. Body temperature was maintained at 37.5°C using a feedback controlled homeothermic heating pad. For all imaging experiments, eyelashes were trimmed and a thin coat of silicone oil (30,000 cSt; Dow Corning) was placed over the eyes for protection.

Two-Photon Calcium Imaging

Two weeks prior to imaging, transplant recipients were injected with AAV-Syn-GCaMP6s (UPenn Vector Core AV-1-PV2824; supplied by the GENIE Project, Janelia Farm Research Campus, HHMI) into binocular visual cortex (2× 150–250 nL, 10 nL/min) using a custom-designed hydraulic injection system. One to two days before imaging, custom made titanium headplates were affixed to the skull using Vet bond and dental acrylic. The skull over visual cortex was thinned to ~50 μm using a dental drill with a carbide burr and a bendable microblade (Nordland Blades #6900).

Intrinsic Imaging

Surgical preparation was performed as previously described (Kaneko et al., 2008). The skull over visual cortex was exposed and covered with agarose (1.5% w/v in 1× PBS) and a coverslip. Agarose was sealed using sterile ophthalmic ointment (Rugby) to prevent drying. For adult MD experiments, monocular deprivation was initiated at the conclusion of pre-MD imaging. Four days later, the sutured eyelid was opened and the skull was exposed at the same location for the second recording session.

Visual Stimuli

Visual stimuli were generated by custom-written Matlab code using the Psychophysics Toolbox (Brainard, 1997). All visual stimuli were confined to −5° to +15° visual field azimuth (binocular visual field). The monitor was positioned 25 cm from the animal and covered with a color correction gel filter sheet (day blue gel D2-70; Lowel) to better exploit the spectral sensitivity of mouse vision (Jacobs et al., 2004).

Calcium Imaging of Orientation Selectivity

Drifting square wave gratings (0.05 cpd; 1 Hz) were presented at 12 orientations using an Acer V193 monitor (30 × 37 cm, 60 Hz refresh rate, 20 cd/m^2 mean luminance). Each trial consisted of 6 s of drifting gratings followed by 6 s of gray screen. Four repeats at each orientation were presented in a pseudorandomized order.

Mapping Binocular Visual Cortex and Assessing Ocular Dominance

Responses to stimulation of the contralateral (previously deprived) versus the ipsilateral eye were recorded from the visual cortex that received transplantation. A visual noise stimulus was presented periodically sweeping either up or down from –18° to 36° visual field elevation. The stimulus was created by multiplying a band limited (<0.05 cyc/degree; >2 Hz) spatiotemporal noise movie with a one dimensional Gaussian spatial mask (20°) that was phase modulated at 0.1 Hz. For adult MD experiments, stimuli were presented on an Acer V193 monitor (30 × 37 cm, 60 Hz refresh rate, 20 cd/m^2 mean luminance). The stimulus was presented for 5 min to each eye in an alternating pattern. One set of recordings was made each at 0° and 180° for four to six sets resulting in a total of 40–60 min (four to six presentations of stimulus movie per eye).

Assessing Acuity of Cortical Responses

For these experiments only responses to stimulation of the contralateral eye were recorded from both the recipient and control hemisphere. Horizontal sinusoidal gratings were presented. These gratings reversed in contrast with a 0.1 Hz sinusoidal modulation. The spatial frequencies of gratings shown were 0.05, 0.1, 0.2, 0.3, 0.4, 0.45, 0.5, 0.55, 0.6, and 0.7 cpd. A grating stimulus at 2 cpd, well in excess of the mouse's visual acuity (Prusky and Douglas, 2003; Prusky et al., 2000), was also presented in order to define background noise. Stimuli were presented on an Asus VG248 monitor (30 × 53 cm, 144 Hz refresh rate, 35 cd/m^2 mean luminance). Recording sessions were performed separately in the recipient hemisphere for deprived eye stimulation and control hemisphere for nondeprived eye stimulation. One to two recordings were made at each spatial frequency for 5 min, totaling 2–4 hr of recording.

Imaging Procedures

Transcranial, Repeated Intrinsic Signal Optical Imaging

Mapping of the primary visual cortex using Fourier intrinsic signal optical imaging was performed through the intact skull as described previously (Kalatsky and Stryker, 2003; Kaneko et al., 2008; Southwell et al., 2010). For adult MD experiments, a custom-designed macroscope (Nikon 135 × 50 mm lenses) equipped with a Dalsa 1M30 CCD camera was used to collect 512 × 512 pixel images sampled at 7.5 Hz (2.2 × 2.2 mm image area). For visual deficit rescue experiments, a SciMedia THT macroscope (Leica PlanApo 1.0X; 3.4 × 3.4 mm image area) equipped with an Andor Zyla sCMOS camera was used. The surface vasculature was visualized using a 530 nm LED light and intrinsic signal

was visualized using a 617 nm LED light (Quadica for MD experiments; Thorlabs LED4D210 for visual deficit rescue experiments). For intrinsic signal recording in both adult MD and visual deficit rescue experiments, the camera was focused ~600 μm beneath the pial surface. Custom written Matlab (Mathworks) code was used to acquire images and stream to disk. Visual stimuli (described above) were presented and response data were collected in 5 min sessions.

Two-Photon Imaging of Calcium Signals

A Sutter MOM system was used to perform two-photon imaging of GCaMP6s and tdTomato fluorescence using 920 nm excitation light (Mai Tai eHP DeepSee). Image sequences typically covering a field of 140 × 140 μm (128 × 128 pixels) were acquired (6.1 Hz) using ScanImage software (v3.8) (Pologruto et al., 2003) at a depth of 150–300 μm below the pia. Red (Chroma HQ605/75) and green (Chroma 565 dcxr) fluorescence emission channels were gathered using a 40× 0.8 NA IR objective (Olympus).

Visual Water Task

Visual acuity was assessed in a visual water maze, a forced choice, two-alternative discrimination task (Prusky and Douglas, 2003). Acuity was determined through each eye independently. A post was surgically implanted onto the skull of each mouse using dental acrylic to act as an attachment point for removable custom-made eye occluders. One week later, mice were trained and tested by an experimenter who was blind to experimental condition. Mice learned to swim toward a hidden platform cued by vertical sine wave gratings displayed at a spatial frequency of 0.063 cpd as viewed from the choice plane (Figure 6A). Mice were trained until they reached performance levels of 90%–100%. Mice then completed testing one eye at a time. During testing, the stimulus was increased by 0.032 cpd when a mouse achieved at least 70% correct over ten trials. Mice were required to successfully complete three trials at frequencies below 0.28 cpd in order to advance. At frequencies above 0.28 cpd they were required to complete five trials successfully in order to advance. If an error was made, they were required to complete a block of 10. When performance fell below 70%, the stimulus was decreased by at least 0.096 cpd. Testing took around 200–250 trials to complete.

Histological Preparation and Cell Counting

Animals were transcardially perfused with saline and 4% paraformaldehyde. Brains were removed, post fixed, and cryoprotected with 30% sucrose. Coronal brain sections (30 or 50 μm) were cut using a frozen sliding microtome (Microm HM450). Tissue was stained in free floating sections. Sections were blocked for 1 hr at room temperature with 0.5% Triton-X (Sigma T8787) and 10% BSA (Fisher BP1600-100) in 1× PBS, then incubated overnight at 4°C with the following primary antibodies: rabbit anti-tdTomato, 1:1,000 (Abcam ab62341); mouse anti-PV, 1:1,000 (Sigma P3088); rat anti-SOM, 1:500 (Millipore MAB354), and rabbit anti-VIP, 1:200 (ImmunoStar). Sections were then washed three times in 1× PBS and incubated for 2 hr at room temperature with fluorescein-labeled wisteria fluorubunda agglutinin at 1:500 (Vector Labs FL-1351) and/or secondary antibodies from Invitrogen at 1:1,000 (goat anti-rat IgG, goat anti-mouse IgG1, goat anti-rabbit IgG). Stained sections were mounted on glass slides with Fluoroshield containing DAPI (Sigma F6057), coverslipped, and imaged using an epifluorescence microscope (Zeiss Axio Imager 2) with a 20× objective (0.8 NA). For cell counting, sections of recipient visual cortex were sampled at 200 or 300 μm intervals. In order to assess the number of transplanted cells in recipient brains, all cells that were tdTomato positive and judged to possess a neuronal morphology were tallied.

Data Analysis

Orientation Selectivity of Cellular Responses

Custom-written Python routines were used to remove motion artifact, identify cell ROIs, extract calcium fluorescence traces, and perform analyses. Transplanted PV+ cells were identified by the expression of tdTomato. The fluorescence signal of a cell body at time t was determined as $F_{cell}(t) = F_{soma}(t) - (R \times F_{neuropil}(t))$ (Chen et al., 2013; Kerlin et al., 2010). R was empirically determined to be 0.7. The neuropil signal $F_{neuropil}(t)$ of each cell was measured by averaging the signal of all pixels outside of the cell and within a 20 μm region from the cell center. In order to quantify orientation responses, each fluorescence trace recorded during the 6 s stimulus presentation was normalized to the average baseline signal for the preceding 3 s ($\Delta F/F_0$). For each orientation condition, a response was computed by taking the average of the normalized fluorescence traces during the stimulus presentation. From these orientation-specific responses, an orientation selectivity index (OSI) was quantified as $(R_{pref} - R_{orth})/(R_{pref} + R_{orth})$, where R_{pref} is the largest response and R_{orth} is the response observed at the orthogonal angle to the preferred response (Niell and Stryker, 2008). Cells that responded to the preferred orientation with an average $\Delta F/F_0$ below 6% were determined nonresponsive and excluded from analysis (4/125).

Intrinsic Signal Imaging

Maps of amplitude and phase of cortical responses were extracted from optical imaging movies via Fourier analysis of each pixel column at the frequency of stimulus repetition (0.1 Hz) (Kalatsky and Stryker, 2003; Southwell et al., 2010) using custom written Matlab code. Overall map amplitude was computed by taking the maximum of the Fourier amplitude map smoothed with a 5 × 5 Gaussian kernel. Maps of retinotopic phase are shown in terms of visual field angle.

Quantification of Ocular Dominance

Ocular dominance index (ODI) was computed as ODI = (C − I)/(C + I) where C and I are the averaged map amplitudes calculated for contralateral and ipsilateral visual stimulation, respectively. Ocular dominance shift (ODS) was calculated for each animal in the adult MD experiments as ODS = (post-MD ODI – pre-MD ODI).

Quantification of Acuity of Visual Cortical Responses

Responses at the following spatial frequencies were recorded for each animal: 0.05, 0.1, 0.2, 0.3, 0.4, 0.45, 0.5, 0.55, 0.6, 0.7, and 2 cpd. For each recording session, the amplitude of the visual response map to 2 cpd was subtracted from the response amplitudes of maps for all other spatial frequencies. For each animal, the highest response to stimulation of the nondeprived eye was taken as 100%, and all other responses were normalized with respect to this value.

Quantification of Cortical Visual Acuity Thresholds

Background noise was taken as the average amplitude of the visual response map to 2 cpd, a stimulus well beyond the limit of mouse spatial acuity. It was determined that the average background noise amplitude (1.52 ± 0.08 $\Delta F/F \times 10^4$) was ~20% of the average peak amplitude of the response (7.3 ± 0.64 $\Delta F/F \times 10^4$). Based on this we determined the threshold of acuity to be the stimulus spatial frequency at which responses fell below 20% (background level) of an animal's nondeprived eye maximum response.

Determination of Perceptual Acuity from Performance on Visual Water Task

Performance on the water task with stimuli of varying spatial frequency was recorded over 200–250 trials as percent correct at a given frequency. The threshold of acuity was determined by the spatial frequency corresponding to the 70% value of the sigmoidal fit to performance data (see Figure 6B) (Prusky et al., 2000).

Statistical Analyses

A one-way ANOVA using Tukey's correction for multiple comparisons was used to compare the mean rank of all groups and determine the differences in the orientation selectivity of transplanted and endogenous PV+ and neighboring PV− neurons ($F_{(3,\ 117)} = 17.56$, $p < 0.0001$; t_{PV-} versus t_{PV+}, $p = 0.0002$; t_{PV-} versus e_{PV+}, $p = 0.001$; t_{PV+} versus e_{PV-}, $p < 0.0001$; e_{PV-} versus e_{PV+}, $p < 0.0001$) (Figure 2D).

A Wilcoxin matched pairs signed rank test was used to compare ODI before versus after 4 days MD in each group in the adult MD experiments. Critical period animals, yellow n = 6: W(5) = −21, p = 0.03; MGE 35 DAT, magenta solid n = 9: W(8) = −45; p = 0.0039; untreated, gray n = 7: W(6) = 2.0, p = 0.88; MGE 70 DAT, cyan n = 8: W(7) = −18, p = 0.16; dead MGE, magenta dashed n = 4 W(3) = −3.0, p = 0.75; LGE, black solid n = 5: W(4) = −5.0, p = 0.56; CGE, black dashed, n = 3, W(2) = 0, p > 0.99. Data for two animals in each of the MGE 70 DAT group CGE group, and critical period group had recordings for only the pre-MD time point that are included in the plot, but not the statistical analysis as they lack the matched post MD paired data (Figure 3B).

A Kruskal-Wallis ANOVA was used to determine significance of differences in ocular dominance shifts across groups in the adult MD experiments

$H = 27.12$, $p = 0.0001$. Mean ranks for control groups were compared to mean rank for critical period animals. Significance values were corrected for multiple comparisons using Dunn's test: critical period animals, yellow, n = 5 versus MGE 35 DAT, magenta solid, n = 9: $p > 0.99$; versus untreated, gray n = 7: $p < 0.003$; versus MGE 70 DAT, cyan n = 8: $p = 0.008$; versus dead MGE, magenta stripes n = 4: $p = 0.03$; versus LGE, black n = 5: $p = 0.02$; versus CGE, black crosshatched, n = 5: $p = 0.02$ (Figure 3C).

A paired t test was used to determine differences between shifts (before and after 4 days MD) in contralateral (deprived) and ipsilateral (nondeprived) response amplitudes following monocular deprivation in adult MD experiments. A D'Agostino-Pearson omnibus test for normality and a ROUT test for outliers with Q set to 1% were used to confirm that data satisfied the assumptions of the t test; contra (n = 8) shift: paired t test; $t(7) = 4.83$, $p = 0.0019$; ipsi (n = 8) shift: $t(7) = 0.045$, $p = 0.97$ (Figure 3D).

An unpaired t test was used to assess differences in PV+ cell counts for 35 DAT and 70 DAT MGE recipient groups. No difference between groups was observed (MGE 35 DAT, 262 ± 90 cells versus MGE 70 DAT, 430 ± 112, $t(9) = 1.02$, $p = 0.34$). Insignificant numbers of PV+ cells were observed in LGE recipients, 42 ± 34 cells.

A linear regression and correlation analysis were used to determine whether there was a linear relationship between number of transplanted PV+ neurons and degree of plasticity induced in MGE cell recipients: $R^2 = 0.042$, $F_{(1,13)} = 0.57$, $p = 0.46$ (Figure 4).

An analysis of covariance (ANCOVA) was used to determine significance of differences between slopes and intercepts (intercepts were not assessed when slopes were too different for accurate assessment) of all linear regression lines in visual deficit rescue experiments; live MGE deprived eye 15 DAT (n = 6) versus 55 DAT (n = 5): slope, $F_{(1,151)} = 6.52$, $p = 0.01$. Dead MGE deprived eye 15 DAT(n = 3) versus 55 DAT(n = 3): slope, $F_{(1,66)} = 3.37$, $p = 0.07$; intercept, $F_{(1,67)} = 0.027$, $p = 0.87$, n.s. (Figures 5D and 5E); MGE deprived 55 DAT (n = 5) versus nondeprived 15 DAT (n = 6): slope, $F_{(1,151)} = 0.055$, $p = 0.82$; intercept, $F_{(1,152)} = 1.34$, $p < 0.25$. MGE deprived (n = 6) versus nondeprived (n = 4) eye 55 DAT: slope, $F_{(1,136)} = 0.278$, $p = 0.6$; intercept, $F_{(1,137)} = 6.44$, $p = 0.99$; MGE deprived 15 DAT versus untreated impaired animals at P170: slope, $F_{(1,116)} = 1.30$, $p = 0.26$; intercept, $F_{(1,117)} = 0.34$, $p = 0.56$; dead MGE deprived versus live MGE deprived 55 DAT: slope, $F_{(1,116)} = 10.52$, $p = 0.002$; deprived eye 0 DAT versus 19-24 DAT: slope, $F_{(1,101)} = 0.56$, $p = 0.46$; intercept, $F_{(1,102)} = 2.86$, $p = 0.09$ (Figure S5).

Kruskal-Wallis ANOVA was used to determine significance of differences in cortical visual acuity for the following: nondeprived eye (15 and 55 DAT assessments averaged) versus deprived eye 15 DAT (live and dead MGE values averaged), live MGE deprived eye 55 DAT, dead MGE deprived eye 55 DAT, and deprived eye in untreated impaired animals (~P170). $H = 28.35$, $p < 0.0001$. Mean rank for each group was compared to mean rank for the nondeprived eye. Significance values were corrected for multiple comparisons using Dunn's test: nondeprived eye (n = 18, green) versus recovery of deprived eye in live MGE recipients 55 DAT (magenta solid, n = 5) $p > 0.99$; versus deprived eye MGE recipients 15 DAT (black, n = 7) $p = 0.002$; versus deprived eye in dead MGE recipients 55 DAT (magenta stripes, n = 3) $p = 0.04$; versus deprived eye in untreated impaired animals ~P170 (gray, n = 4), $p = 0.03$ (Figure 5F).

An ordinary one-way ANOVA was used to determine significance of differences perceptual visual acuity for the deprived and nondeprived eyes from both recipients and nonrecipients as well as from naive animals that were never deprived and received no treatment (MGE recipients deprived eye, n = 5; nonrecipients deprived eye, n = 9; nondeprived eyes, n = 18; naive animals, n = 9), $F_{(3,\ 37)} = 7.52$, $p = 0.0005$. Mean rank for each group was compared to mean rank for each other group. Significance values were corrected for multiple comparisons using Tukey's test; MGE recipient deprived eye versus nondeprived eye, $p = 0.97$; MGE recipient deprived eye versus nonrecipient deprived eye, $p = 0.007$; MGE recipient deprived eye versus naive animal, $p = 0.99$; nonrecipient deprived eye versus nondeprived eye, $p = 0.0008$; nonrecipient deprived eye versus naive animals, $p = 0.003$; nondeprived eye versus naive animals, $p = 1.0$ (Figure 6C).

A paired Mann-Whitney test was used to determine significance of differences in maximum performance on the behavioral task for the nondeprived eye in impaired animals versus naive controls. Normal performance using the nondeprived eye confirmed that each animal was capable of performing the task and that the acuity deficit observed was specific to the deprived eye ($U(11) = 12.50$, $p = 0.21$; Figure 6B, middle, inset graph).

All error was reported or plotted as SEM. All statistical analyses were performed using Prism 6.03 (Graphpad).

SUPPLEMENTAL INFORMATION

Supplemental Information includes five figures and can be found with this article at http://dx.doi.org/10.1016/j.neuron.2015.03.062.

AUTHOR CONTRIBUTIONS

M.F.D., D.X.F.-V., and S.P.G. designed the experiments. D.X.F.-V. performed the transplantation procedures with support from M.F.D and M.C.Y. D.X.F.-V. recorded and analyzed two-photon calcium imaging data. M.F.D. made intrinsic signal recordings and analyzed optical imaging data. R.P.G. trained and tested mice on the visual task. M.C.C. developed acquisition and analysis routines for the two-photon and optical imaging experiments. D.X.F.-V. and M.H. prepared tissue for histology and performed histological analysis. M.F.D., D.X.F.-V., and S.P.G. wrote the manuscript.

ACKNOWLEDGMENTS

We are grateful to D. Agalliu for advice and training on histological procedures and to I. Villano for assistance with histological preparation. We would like to thank K. Ellefsen for providing calcium imaging analysis routines. We would also like to thank C. Neill and D. Southwell for providing a critical reading of the manuscript. This work was supported by a NIH Director's New Innovator Award (DP2 EY024504-01), a Searle Scholars Award, and a Klingenstein Fellowship. M.F.D. was supported by a postdoctoral training grant from the California Institute for Regenerative Medicine (TG2-01152).

Received: October 2, 2014
Revised: February 6, 2015
Accepted: March 23, 2015
Published: April 30, 2015

REFERENCES

Beurdeley, M., Spatazza, J., Lee, H.H.C., Sugiyama, S., Bernard, C., Di Nardo, A.A., Hensch, T.K., and Prochiantz, A. (2012). Otx2 binding to perineuronal nets persistently regulates plasticity in the mature visual cortex. J. Neurosci. *32*, 9429–9437.

Brainard, D.H. (1997). The psychophysics toolbox. Spat. Vis. *10*, 433–436.

Chen, T.-W., Wardill, T.J., Sun, Y., Pulver, S.R., Renninger, S.L., Baohan, A., Schreiter, E.R., Kerr, R.A., Orger, M.B., Jayaraman, V., et al. (2013). Ultrasensitive fluorescent proteins for imaging neuronal activity. Nature *499*, 295–300.

Fagiolini, M., and Hensch, T.K. (2000). Inhibitory threshold for critical-period activation in primary visual cortex. Nature *404*, 183–186.

Fagiolini, M., Fritschy, J.-M., Löw, K., Möhler, H., Rudolph, U., and Hensch, T.K. (2004). Specific GABAA circuits for visual cortical plasticity. Science *303*, 1681–1683.

Fu, Y., Kaneko, M., Tang, Y., Alvarez-Buylla, A., and Stryker, M.P. (2015). A cortical disinhibitory circuit for enhancing adult plasticity. Elife *4*.

Heimel, J.A., Hartman, R.J., Hermans, J.M., and Levelt, C.N. (2007). Screening mouse vision with intrinsic signal optical imaging. Eur. J. Neurosci. *25*, 795–804.

Hensch, T.K. (2005). Critical period plasticity in local cortical circuits. Nat. Rev. Neurosci. *6*, 877–888.

Hensch, T.K., Fagiolini, M., Mataga, N., Stryker, M.P., Baekkeskov, S., and Kash, S.F. (1998). Local GABA circuit control of experience-dependent plasticity in developing visual cortex. Science *282*, 1504–1508.

Hippenmeyer, S., Vrieseling, E., Sigrist, M., Portmann, T., Laengle, C., Ladle, D.R., and Arber, S. (2005). A developmental switch in the response of DRG neurons to ETS transcription factor signaling. PLoS Biol. *3*, e159.

Huang, Z.J., Kirkwood, A., Pizzorusso, T., Porciatti, V., Morales, B., Bear, M.F., Maffei, L., and Tonegawa, S. (1999). BDNF regulates the maturation of inhibition and the critical period of plasticity in mouse visual cortex. Cell *98*, 739–755.

Jacobs, G.H., Williams, G.A., and Fenwick, J.A. (2004). Influence of cone pigment coexpression on spectral sensitivity and color vision in the mouse. Vision Res. *44*, 1615–1622.

Kalatsky, V.A., and Stryker, M.P. (2003). New paradigm for optical imaging: temporally encoded maps of intrinsic signal. Neuron *38*, 529–545.

Kaneko, M., and Stryker, M.P. (2014). Sensory experience during locomotion promotes recovery of function in adult visual cortex. Elife *3*, e02798.

Kaneko, M., Hanover, J.L., England, P.M., and Stryker, M.P. (2008). TrkB kinase is required for recovery, but not loss, of cortical responses following monocular deprivation. Nat. Neurosci. *11*, 497–504.

Kerlin, A.M., Andermann, M.L., Berezovskii, V.K., and Reid, R.C. (2010). Broadly tuned response properties of diverse inhibitory neuron subtypes in mouse visual cortex. Neuron *67*, 858–871.

Kuhlman, S.J., Tring, E., and Trachtenberg, J.T. (2011). Fast-spiking interneurons have an initial orientation bias that is lost with vision. Nat. Neurosci. *14*, 1121–1123.

Kuhlman, S.J., Olivas, N.D., Tring, E., Ikrar, T., Xu, X., and Trachtenberg, J.T. (2013). A disinhibitory microcircuit initiates critical-period plasticity in the visual cortex. Nature *501*, 543–546.

Lehmann, K., and Löwel, S. (2008). Age-dependent ocular dominance plasticity in adult mice. PLoS ONE *3*, e3120.

Li, Y.-T., Ma, W.-P., Pan, C.-J., Zhang, L.I., and Tao, H.W. (2012). Broadening of cortical inhibition mediates developmental sharpening of orientation selectivity. J. Neurosci. *32*, 3981–3991.

Madisen, L., Zwingman, T.A., Sunkin, S.M., Oh, S.W., Zariwala, H.A., Gu, H., Ng, L.L., Palmiter, R.D., Hawrylycz, M.J., Jones, A.R., et al. (2010). A robust and high-throughput Cre reporting and characterization system for the whole mouse brain. Nat. Neurosci. *13*, 133–140.

Maya Vetencourt, J.F., Sale, A., Viegi, A., Baroncelli, L., De Pasquale, R., O'Leary, O.F., Castrén, E., and Maffei, L. (2008). The antidepressant fluoxetine restores plasticity in the adult visual cortex. Science *320*, 385–388.

Miyoshi, G., Hjerling-Leffler, J., Karayannis, T., Sousa, V.H., Butt, S.J.B., Battiste, J., Johnson, J.E., Machold, R.P., and Fishell, G. (2010). Genetic fate mapping reveals that the caudal ganglionic eminence produces a large and diverse population of superficial cortical interneurons. J. Neurosci. *30*, 1582–1594.

Montey, K.L., Eaton, N.C., and Quinlan, E.M. (2013). Repetitive visual stimulation enhances recovery from severe amblyopia. Learn. Mem. *20*, 311–317.

Niell, C.M., and Stryker, M.P. (2008). Highly selective receptive fields in mouse visual cortex. J. Neurosci. *28*, 7520–7536.

Pla, R., Borrell, V., Flames, N., and Marín, O. (2006). Layer acquisition by cortical GABAergic interneurons is independent of Reelin signaling. J. Neurosci. *26*, 6924–6934.

Pologruto, T.A., Sabatini, B.L., and Svoboda, K. (2003). ScanImage: flexible software for operating laser scanning microscopes. Biomed. Eng. Online *2*, 13.

Prusky, G.T., and Douglas, R.M. (2003). Developmental plasticity of mouse visual acuity. Eur. J. Neurosci. *17*, 167–173.

Prusky, G.T., West, P.W., and Douglas, R.M. (2000). Behavioral assessment of visual acuity in mice and rats. Vision Res. *40*, 2201–2209.

Runyan, C.A., and Sur, M. (2013). Response selectivity is correlated to dendritic structure in parvalbumin-expressing inhibitory neurons in visual cortex. J. Neurosci. *33*, 11724–11733.

Runyan, C.A., Schummers, J., Van Wart, A., Kuhlman, S.J., Wilson, N.R., Huang, Z.J., and Sur, M. (2010). Response features of parvalbumin-expressing interneurons suggest precise roles for subtypes of inhibition in visual cortex. Neuron *67*, 847–857.

Sato, M., and Stryker, M.P. (2008). Distinctive features of adult ocular dominance plasticity. J. Neurosci. *28*, 10278–10286.

Sawtell, N.B., Frenkel, M.Y., Philpot, B.D., Nakazawa, K., Tonegawa, S., and Bear, M.F. (2003). NMDA receptor-dependent ocular dominance plasticity in adult visual cortex. Neuron *38*, 977–985.

Southwell, D.G., Froemke, R.C., Alvarez-Buylla, A., Stryker, M.P., and Gandhi, S.P. (2010). Cortical plasticity induced by inhibitory neuron transplantation. Science *327*, 1145–1148.

Southwell, D.G., Nicholas, C.R., Basbaum, A.I., Stryker, M.P., Kriegstein, A.R., Rubenstein, J.L., and Alvarez-Buylla, A. (2014). Interneurons from embryonic development to cell-based therapy. Science *344*, 1240622.

Stephany, C.-É., Chan, L.L.H., Parivash, S.N., Dorton, H.M., Piechowicz, M., Qiu, S., and McGee, A.W. (2014). Plasticity of binocularity and visual acuity are differentially limited by nogo receptor. J. Neurosci. *34*, 11631–11640.

Sugiyama, S., Di Nardo, A.A., Aizawa, S., Matsuo, I., Volovitch, M., Prochiantz, A., and Hensch, T.K. (2008). Experience-dependent transfer of Otx2 homeoprotein into the visual cortex activates postnatal plasticity. Cell *134*, 508–520.

Tang, Y., Stryker, M.P., Alvarez-Buylla, A., and Espinosa, J.S. (2014). Cortical plasticity induced by transplantation of embryonic somatostatin or parvalbumin interneurons. Proc. Natl. Acad. Sci. USA *111*, 18339–18344.

Tognini, P., Manno, I., Bonaccorsi, J., Cenni, M.C., Sale, A., and Maffei, L. (2012). Environmental enrichment promotes plasticity and visual acuity recovery in adult monocular amblyopic rats. PLoS ONE *7*, e34815.

Vong, L., Ye, C., Yang, Z., Choi, B., Chua, S., Jr., and Lowell, B.B. (2011). Leptin action on GABAergic neurons prevents obesity and reduces inhibitory tone to POMC neurons. Neuron *71*, 142–154.

Wichterle, H., Garcia-Verdugo, J.M., Herrera, D.G., and Alvarez-Buylla, A. (1999). Young neurons from medial ganglionic eminence disperse in adult and embryonic brain. Nat. Neurosci. *2*, 461–466.

Wonders, C.P., and Anderson, S.A. (2006). The origin and specification of cortical interneurons. Nat. Rev. Neurosci. *7*, 687–696.